



UKAEA-CCFE-PR(25)373

Wayne Arter

Spiking without and with blue-sky catastrophe

Enquiries about copyright and reproduction should in the first instance be addressed to the UKAEA Publications Officer, Culham Science Centre, Building K1/0/83 Abingdon, Oxfordshire, OX14 3DB, UK. The United Kingdom Atomic Energy Authority is the copyright holder.
The contents of this document and all other UKAEA Preprints, Reports and Conference Papers are available to view online free at scientific-publications.ukaea.uk/

Spiking without and with blue-sky catastrophe

Wayne Arter

SPIKING WITHOUT AND WITH BLUE-SKY CATASTROPHE

WAYNE ARTER

Computing Division, United Kingdom Atomic Energy Authority, Culham Campus, Abingdon, Oxfordshire. OX14 3DB wayne.arter@ukaea.uk

Received (to be inserted by publisher)

Two closely-related candidate surrogate models for global tokamak plasma dynamics both exhibit spiking behaviour, which may be understood using concepts from the classical problem of particle motion in a well of potential energy. Numerical work indicates that when there is coupled evolution of the well's properties, an attractor appears which has properties resembling those of the blue-sky catastrophe. However, the attractor has unusual features attributable to a lack of dissipation in the model. The simplicity of the models is remarked upon and implications for the understanding of spiking activity generally are discussed.

Keywords: spiking, blue-sky catastrophe, bifurcation, tokamak.

1. Introduction

Spiking activity consists of sets of 'spikes' that are defined as abrupt and transient changes in system output [Izhikevich, 2007, § 1]. With that definition, spikes are seen not only in the neuroscience of the human brain, but also in certain aspects of global behaviour of plasma in magnetic confinement fusion devices such as tokamaks and reversed field pinches, and of solar plasma in recurrent flaring events [Yamada, 2022]. Herein 'abrupt' will be taken to mean exponentially growing, and Izhikevich's approach implicitly assumes that the 'change' is occurring close to an instability threshold, which ideas inform the dynamical systems treatment adopted herein. Recent references [Kuptsov et al., 2017], [Gonchenko et al., 2022] and [Sanaullah et al., 2023] show continuing widespread interest in problems of spiking activity, sometimes extending to blue-sky bifurcation.

The ANAC (Axisymmetric/Non-Axisymmetric Coupled) model for global tokamak plasma dynamics was introduced by [Arter, 15 May 2009] in view of earlier considerations [Arter, 2009]. Those references argue that the simplest, plausible nonlinear model satisfying certain symmetry constraints couples a (non-axisymmetric) mode with amplitude a satisfying

$$\ddot{a} = \gamma_r a + 2\mu_r a^3 \tag{1}$$

to an equation for a second (axisymmetric) mode of amplitude b

$$\dot{b} = \nu_1 - \nu_2 b^2 - (1 + \delta_r b) a^2 \tag{2}$$

where over-dot denotes time derivative, a(t) and b(t) are both real functions of time t, and γ_r , $2\mu_r$, ν_1 , ν_2 , and δ_r are real, but not necessarily arbitrary parameters.

Sample calculations show spiky oscillations in variable a(t) which for large negative coupling coefficient δ_r produce huge spikes in the behaviour of b(t). Consistent with a sawtooth-like effect at smaller δ_r ,

these b-spikes are asymmetric, with a faster rate of rise than fall-off, see Section 2.1. Many other tokamak plasma models of varying degrees of complexity are at least as plausible, motivating the making of a fit of the above equivariant-bifurcation-theory inspired model to experimental time series data. Eqs.(1) and (2) are based on a topological normal form for the expected flow in the 3-D phase space (a, \dot{a}, b) . In the normal form the parameters $2\mu_r = \pm 1$, $\nu_2 = 1$ are to be regarded as fixed, and the term in δ_r introduced above is not required. Despite the generalisation, an attempt to fit the model directly to experimental data might be defeated by the sparseness of ANAC above.

Such a consideration led to the more complicated ANAET (Axisymmetric/Non-Axisymmetric coupled Extra Terms) systems. Possible extensions include back-coupling of the axisymmetric mode to the mode a, higher odd-order terms in Eq. (1), coupling to further modes and terms representing symmetry-breaking perturbations. For present purposes it is sufficient to consider only the first two extensions, giving ANAET as

$$\ddot{a} = -\gamma_0 a + (\mu_2 b - \mu_1) a^3 - \mu_6 a^6 \dot{a} \tag{3}$$

$$\dot{b} = \nu_1 - \nu_2 b^2 + (\delta_1 b - \delta_0) a^2 \tag{4}$$

where γ_0 , μ_j , ν_j and δ_j are arbitrary real parameters, although with the choice of signs in Eqs.(3) and (4), all are normally to be taken as positive, except that frequently $\mu_1 = \delta_1 = 0$. The 'extra term' appearing when $\mu_6 \neq 0$ is purely inspired by physical considerations, designed to introduce damping only at large |a|. The term ensures that |a| and |b| remain bounded, allowing behaviour described in Section 2.3 suggesting the existence of a blue-sky catastrophe as described in Section 2.4. The implications of these results and others from Section 2 for spiking activity are discussed in the concluding Section 3.

2. Analysis and Computation

2.1. ANAC Model

Considering first Eq. (1) on its own, the solution for the time dependent amplitude a(t) may be given explicitly as an elliptic function. The best way to establish this relationship analytically seems to be to integrate Eq. (1) with respect to (w.r.t.) time once, giving

$$\dot{a}^2 = 2H + \gamma_r a^2 + \mu_r a^4 \tag{5}$$

where H is a constant of integration which is determined by the initial values of a and \dot{a} ,

$$H = \frac{1}{2}(\dot{a}^2 - \gamma_r a^2 - \mu_r a^4)|_{t=0}$$
(6)

Eq. (5) implies that a corresponds to the motion of the position of a particle in a potential

$$2V(a) = -\gamma_r a^2 - \mu_r a^4 \tag{7}$$

This potential is illustrated for positive values of $(-\mu_r)$ in Fig. 1.

Among the many textbooks which define Jacobi elliptic functions, a convenient reference for current purposes is [Gradshteyn and Ryzhik, 1980]. From ref [Gradshteyn and Ryzhik, 1980, § 8.159]), the Jacobi cn(u|k) function satisfies the equation

$$\left(\frac{dy}{du}\right)^2 = (1 - y^2)(1 - k^2 + k^2y^2) \tag{8}$$

and the Jacobi dn(u|k) function satisfies

$$\left(\frac{dy}{du}\right)^2 = (1 - y^2)(y^2 - 1 + k^2) \tag{9}$$

where in both cases, the modulus k must satisfy |k| < 1. It follows that $y = Ccn(\lambda(t - t_0)|k)$ satisfies

$$\dot{y}^2 = C^2 \lambda^2 (1 - \frac{y^2}{C^2})(1 - k^2 + k^2 \frac{y^2}{C^2}) \tag{10}$$

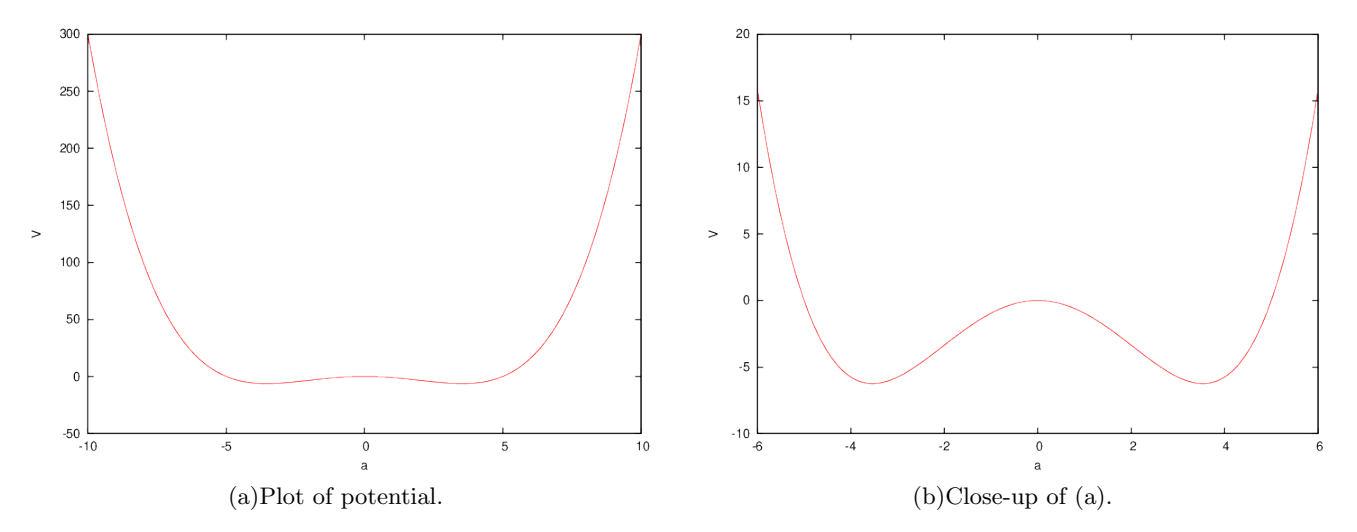


Fig. 1. Potential determining amplitude evolution of a, for parameters $\gamma_r = 1$ and $-\mu_r = 0.04$.

which may be expanded as

$$\dot{y}^2 = C^2 \lambda^2 (1 - k^2) + \lambda^2 (2k^2 - 1)y^2 - \frac{\lambda^2 k^2}{C^2} y^4 \tag{11}$$

Similarly $y = Cdn(\lambda(t-t_0)|k)$ satisfies

$$\dot{y}^2 = -C^2 \lambda^2 (1 - k^2) + \lambda^2 (2 - k^2) y^2 - \frac{\lambda^2}{C^2} y^4$$
(12)

The comparison between Eq. (5) and Eqs.(11) and (12) shows that if H > 0, a must be of cnoidal (cn)form and

$$k^2 = 1 - \frac{2H}{C^2 \lambda^2} \tag{13}$$

whereas if H < 0, $a = Cdn(\lambda(t - t_0)|k)$ is dnoidal, where

$$k^2 = 1 + \frac{2H}{C^2 \lambda^2} \tag{14}$$

Referring to Fig. 1, small positive values of H correspond to a small value of energy of motion, and oscillations which change sign (cn function), small negative values to oscillations over the width of one of the two potential wells (dn function).

Equations for C and λ in terms of γ_r and μ_r follow from the term-by-comparison of the powers of a (equivalently y) between Eq. (5) and Eqs. (11) and (12) following [Murari et al., 2011]. In the cnoidal case, this comparison gives

$$\lambda^2 (2k^2 - 1) = \gamma_r \quad , \quad \frac{\lambda^2 k^2}{C^2} = -\mu_r$$
 (15)

implying $\mu_r < 0$. Substituting for k^2 from Eq. (13), and eliminating λ between the resulting two equations Eq. (15), gives a quadratic for the square amplitude C^2 , of which the only positive solution is

$$C^{2} = \frac{\gamma_{r} + \sqrt{(\gamma_{r}^{2} + 8(-\mu_{r})H)}}{2(-\mu_{r})}$$
(16)

and it follows that

$$\lambda = \sqrt[4]{(\gamma_r^2 + 8(-\mu_r)H)} \tag{17}$$

and finally that

$$k^2 = 1 - \frac{1}{2} \left(1 - \frac{1}{\sqrt{(1+8h)}} \right) \tag{18}$$

where

$$h = |\mu_r H|/\gamma_r^2 \tag{19}$$

The relevant manipulations for the dnoidal comparison are slightly easier and give

$$C^2 = \lambda^2 / (-\mu_r) \tag{20}$$

where

$$\lambda^2 = \frac{1}{2} \left(\gamma_r + \sqrt{(\gamma_r^2 + 8(-\mu_r)H)} \right) \tag{21}$$

and finally that

$$k^2 = 1 - \frac{4h}{(1-2h) + \sqrt{(1-8h)}} \tag{22}$$

A second initial condition, say specifying a(0), would serve to determine t_0 , but for physical application the origin of time should be unimportant.

Brizard [Brizard, 2009, Fig. 4] illustrates graphically that there is an almost continuous transition at $k^2 = 1$ or H = 0 from a solution of cnoidal form, which reverses sign like say the more familiar cosine function, to a dnoidal solution, which keeps the same sign, and first appears looking like one half-period of the cnoidal solution. This is expected from inspection of Fig. 1, wherein a particle starting close to a at t = 0 will head rapidly into the depth of the nearest well, and if it starts with positive energy will explore each of the two wells in turn. The critical solution, separating reversing from non-reversing periodic solutions, has an 'infinite' period. In topological language, there is a heteroclinic bifurcation at $k^2 = 1$.

As might be expected from the classical problem, and indeed is confirmed by for example the plots Figs 63-4 and 63-5 of [Oldham et al., 2009, p. 641], for values of |k| near unity, the cnoidal and dnoidal functions become most spike-like, see also Fig. 2(a). The asymptotic theory for the large periods P of oscillation for k^2 near critical [Gradshteyn and Ryzhik, 1980, § 8.113(3)], gives

$$P \sim \frac{1}{\lambda} \ln \left(\frac{4}{\sqrt{(1-k^2)}} \right) \simeq \frac{1}{2\sqrt{\gamma_r}} \ln \left(\frac{8}{h} \right)$$
 (23)

on observing that both Eq. (13) and Eq. (14) yield $k^2 \approx 1 - 2h$ in the limit of small h, which from Eq. (19) and Eq. (6) is consistent with small initial values of a and \dot{a} .

Note that the spiky behaviour of elliptics is often missed for two reasons. First, it does not appear for most of the range of allowed values of k. Second, there is a significant feature omitted when dn is introduced analogously to sine or cosine, perhaps best illustrated when the initial condition $\dot{a}=0$ is employed. In the sinusoidal case, this implies that a(0) is the maximum absolute value of a(t), whereas in the dnoidal case, $\dot{a}=0$ might correspond to the minimum value of a(t), which tends to zero as $k^2\to 1$. The maximum value of a(t) is determined by the nonlinearity in the definitions Eqs.(11) and (12) which couples phase of function argument (fixed by initial condition), modulus (the analogue of wavenumber) and amplitude of an elliptic function as indicated above, hence a(t) may subsequently become much larger than a(0), despite $\dot{a}(0)=0$. Although cn may not have vanishing derivative between extrema since H>0, dcn/dt may become vanishingly small when $k^2\to 1$ so a similar disparity between initial condition and maximum (absolute) function value is possible for cn.

Of more novelty is the effect of increased coupling of the elliptic function a(t) into the evolution equation Eq. (4) for b. This was obtained by numerical solution, which like all numerical solutions presented herein was obtained by employing a user-written interface to the LSODE software [Radhakrishnan and Hindmarsh, 1993]. The solver uses a variable-order, variable-step multi-step method, with solution tolerances set to 10^{-12} , about the smallest possible in a double precision numerical implementation. The solutions were sampled every 0.1 time units. At the parameters given, a ranges from zero to approximately 1.4, and Fig. 2 at left shows a relatively minor effects on b typical of small values of $|\delta_r|$. However, for the much larger value of $|\delta_r|$ at right, the same a(t) causes spiking to very large maximum values of |b|.



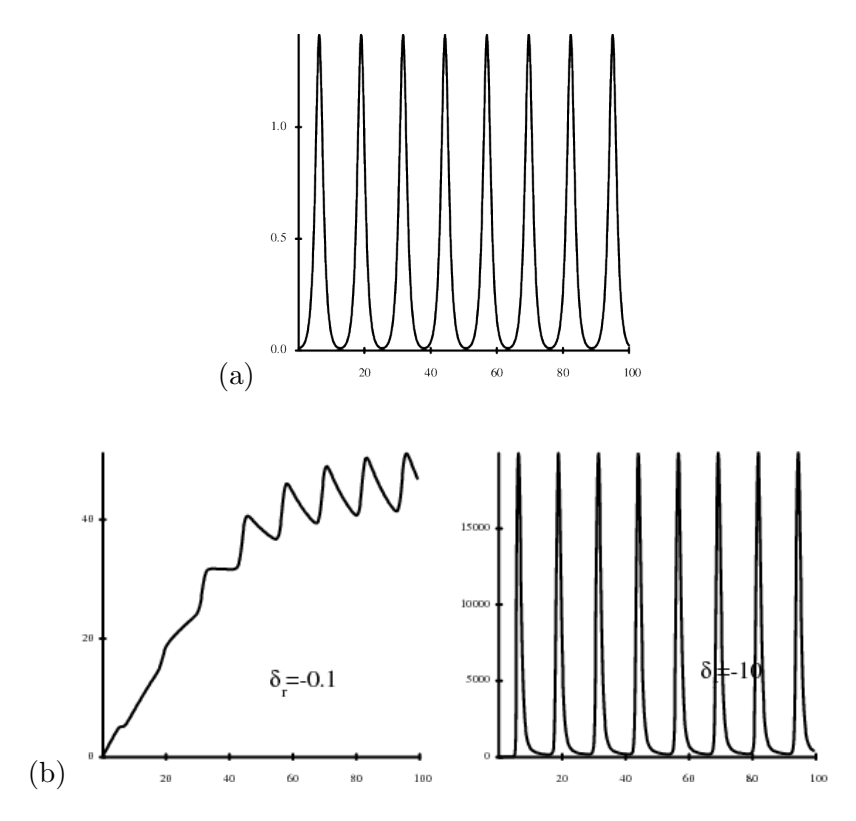


Fig. 2. (a) Elliptic function a(t). (b) Plots of b(t) for the two values of δ_r indicated on the plot. Other parameters $\gamma_r=1$, $2\mu_r=-1$, $\nu_1=1$ and $\nu_2=\epsilon=10^{-3}$. Initial conditions a(0)=0.01, $\dot{a}(0)=b(0)=0$.

2.2. ANAET Model Potential

A crucial difference from Section 2.1 is that whereas the linear term in ANAC was destabilising and the nonlinear term was stabilising, now the linear term on the right-hand-side of the equation for \ddot{a} corresponds to oscillation and the cubic nonlinear term is destabilising if it assumed that γ_0 and μ_1 are both positive. The result of the change is the formation of a potential well as shown in Fig. 3. Even so, in order to keep solutions bounded, it is helpful to have the high order damping term in Eq. (3).

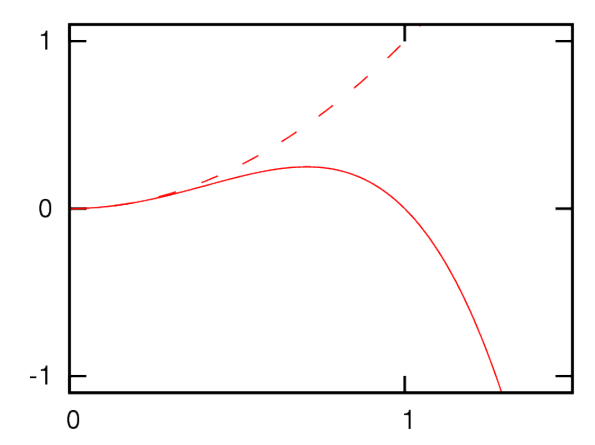


Fig. 3. Sketches of potential V which is symmetric about a=0 as a function of variable a at two different times. The dashed line shows an initial quadratic potential V, and the solid line shows V following the addition of a negative function $\mu_{\tau}a^4$, which has limited the width of the potential well about the origin. Reproduction of ref [Arter, 2011, Fig. 2].

As in the previous ANAC Section 2.1, consider the variation of a on its own, ie. with reference only to Eq. (1). (In Eq. (3), the coupling to b is eliminated simply by setting $\mu_2 = 0$.) Suppose that $\gamma_r = -\gamma_0 = -\omega_o^2$, so that the linear term in Eq. (1) represents oscillation at frequency ω_o . Proceed by calculating the value of $a = a_m$ at the top of the potential well from $V'(a_m) = 0$, giving $a_m^2 = \gamma_0/\mu_1$ then substitute in $V''(a) = \gamma_0 - 3\mu_1 a^2$. The result is $V''(a_m) = -2\gamma_0$ whence it follows that the mode growing from the top of the potential well does so at a rate $\omega_o\sqrt{2}$, ie. faster than the rate of oscillation about a = 0. Thus, if a relatively small change in μ_r with time brings the potential barrier below the energy of the original oscillation (or the energy of the oscillator is somehow correspondingly increased), then there will be rapid growth of the amplitude a.

This result is sufficiently important that it justifies a more formal treatment.

Theorem 1. Escape from a smooth, locally quadratic potential well occurs at an exponential rate at least as fast as the original frequency of oscillation, subject to a relatively unrestrictive condition on the potential function which is stated.

Proof. Write the potential as

$$V(a) = \frac{1}{2}\omega_o^2 a^2 + v_n a^n + r_\ell(a)$$
(24)

where integer $n \geq 3$ and r_{ℓ} is of order a^{ℓ} , $\ell > n$, as might be defined as the remainder of a convergent Taylor expansion about a = 0. Motion in the potential obeys

$$\ddot{a} = -V'(a) = -\omega_o^2 a + n v_n a^{n-1} + r'_{\ell}(a)$$
(25)

where 'dot' denotes differentiation w.r.t. time and 'dash' that the function is to be differentiated w.r.t. its argument. Evidently for sufficiently small a, the higher order terms are negligible and oscillation occurs at a frequency ω_o . Suppose now that the well is of finite extent, admitting escape at $a_m = \mathcal{O}(1)$, the location of the first maximum reached by V so that $V'(a_m) = 0$. Should escape occur at $a = a_m$, linearising Eq. (25)

about a_m , gives the local behaviour as

$$\ddot{\epsilon} = -V''(a_m)\epsilon \tag{26}$$

Since V is a maximum, V'' < 0 and the perturbation ϵ will grow at a rate given by $\sqrt{-V''(a_m)}$. Making use of the explicit form Eq. (24) of V,

$$V'(a_m) = \omega_o^2 a_m + n v_n a_m^{n-1} + r_\ell'(a_m) = 0$$
(27)

$$V''(a_m) = \omega_o^2 + n(n-1)v_n a_m^{n-2} + r_\ell''(a_m)$$
(28)

Substituting for $nv_na_m^{n-2}$ from Eq. (27) into Eq. (28) gives

$$V''(a_m) = \omega_o^2 + (n-1)\left(-\omega_o^2 - \frac{r'_{\ell}(a_m)}{a_m}\right) + r''_{\ell}(a_m)$$
(29)

ie.

$$V''(a_m) = (2 - n)V''(0) + R_{\ell,n}(a_m), \text{ where } R_{\ell,n} = \frac{(a_m r_{\ell}'' - (n - 1)r_{\ell}')}{a_m}$$
(30)

Thus if the estimation $r_{\ell} = v_{\ell} a^{\ell}$ is made,

$$R_{\ell,n} = \ell(\ell - n)v_{\ell}a_m^{\ell - 2} \tag{31}$$

so if $|R_{\ell,n}|$ is small (eg. when v_{ℓ} is negligible), a grows at a rate $\omega_o\sqrt{(n-2)}$ for a near a_m .

In other words, following a blue-sky homoclinic bifurcation the dynamical system has trajectories that are traversed exponentially fast, at rates which have the timescale of the linear frequency of oscillation about the original focus. Insofar as the heteroclinic bifurcation described in Section 2.1 resembles two homoclinic bifurcations, the same result applies to it.

It is worth noting that generally the above approach is superior to making a single Taylor expansion about $a = a_{\mu} = a_m/2$, despite the symmetric choice of location of a. Writing

$$V(a) = V(a_{\mu}) + (a - a_{\mu})V'(a_{\mu}) + \frac{(a - a_{\mu})^{2}}{2!}V''(a_{\mu}) + \sum_{\ell} \frac{(a - a_{\mu})^{\ell}}{\ell!}V^{(\ell)}(a_{\mu}), \quad \ell = 3, 4, \dots$$
 (32)

it follows that

$$V'(0) = V'(a_{\mu}) + \sum_{\ell > 0} (-1)^{\ell} \frac{a_{\mu}^{\ell}}{\ell!} V^{(\ell+1)}(a_{\mu}) = 0$$
(33)

$$V''(0) = V''(a_{\mu}) + \sum_{\ell>0} (-1)^{\ell} \frac{a_{\mu}^{\ell}}{\ell!} V^{(\ell+2)}(a_{\mu})$$
(34)

$$V'(a_m) = V'(a_\mu) + \sum_{\ell>0} \frac{a_\mu^{\ell}}{\ell!} V^{(\ell+1)}(a_\mu) = 0$$
(35)

$$V''(a_m) = V''(a_\mu) + \sum_{\ell>0} \frac{a_\mu^\ell}{\ell!} V^{(\ell+2)}(a_\mu)$$
(36)

Hence adding Eq. (34) and Eq. (36) gives

$$V''(0) + V''(a_m) = 2V''(a_\mu) + 2\Sigma_{\text{even }\ell > 0} \frac{a_\mu^\ell}{\ell!} V^{(\ell+2)}(a_\mu)$$
(37)

Each of Eqs. (33) and (35) has a term in $a_{\mu}V''(a_{\mu})$, which may be eliminated respectively as

$$a_{\mu}V''(a_{\mu}) = -V'(a_{\mu}) - \frac{a_{\mu}^{2}}{2!}V'''(a_{\mu}) - \frac{a_{\mu}^{3}}{3!}V^{(4)}(a_{\mu}) + \dots$$
(38)

$$a_{\mu}V''(a_{\mu}) = +V'(a_{\mu}) + \frac{a_{\mu}^{2}}{2!}V'''(a_{\mu}) - \frac{a_{\mu}^{3}}{3!}V^{(4)}(a_{\mu}) + \dots$$
(39)

Adding Eqs. (38) and (39) and substituting in Eq. (37), gives to leading order

$$V''(0) + V''(a_m) = \frac{2}{3}a_\mu^2 V^{(4)}(a_\mu) + \dots$$
(40)

At first sight Eq. (40) appears to show that $V''(a_m) = -V''(0)$, ie. growth rate at a_m equal to oscillation frequency at a = 0, which is indeed true when V(a) is antisymmetric, V(-a) = -V(a). Unfortunately when this symmetry is lacking, since a_{μ} is in general not small, for the example of motion satisfying $\ddot{a} = -a + a^3$, so $V(a) = \frac{1}{2}a^2 - \frac{1}{4}a^4$, the term on the right-hand-side of Eq. (40) has value unity compared to a frequency $\omega_0 = 1$, ie. 100 % error.

2.3. ANAET and ANAETs Model Properties

Guided by theory and intuition, in order to obtain a sawtooth oscillation with period decoupled from that of the basic ideal oscillator, the idea has been to arrange matters so that the slow growth in b destabilises a, as the term in $\mu_2 b$ changes to produce a different effective μ_r . As just proven above, the result is that a shoots up exponentially fast, pulling b back down to negative values so that the μ_2 term is stabilising once more, and the cycle repeats, to give the kind of biperiodic oscillation illustrated in Fig. 4. Numerical experiment also indicates that to aid analytic understanding, it is helpful to introduce into ANAET a 'slow time' dependent variable $\bar{\tau} = \epsilon t$ and cf. the fast/slow approach of [Diener, 1984], normalise all the coefficients apart from γ_0 , μ_1 and μ_2 by ϵ as follows, $\mu_6 = \epsilon \tilde{\mu_6}$, $\nu_1 = \epsilon \tilde{\nu_1}$, $\nu_2 = \epsilon \tilde{\nu_2}$, $\delta_0 = \epsilon \tilde{\delta_0}$ and $\delta_1 = \epsilon \tilde{\delta_1}$, which recasts the equations as

$$a_{\bar{\tau}\bar{\tau}} = \epsilon^{-2} \left(-\gamma_0 a + [\mu_2 b - \mu_1] a^3 \right) - \tilde{\mu}_6 a^6 a_{\bar{\tau}} \tag{41}$$

$$b_{\bar{\tau}} = \tilde{\nu}_1 - \tilde{\nu}_2 b^2 + (\tilde{\delta}_1 b - \tilde{\delta}_0) a^2 \tag{42}$$

To capture the oscillatory behaviour discovered in Fig. 4, it is adequate to set $\mu_1 = 0$ because a non-zero value principally serves to offset the stabilisation process, for which the additional coupling term in $\tilde{\delta}_1$ is also inessential. The number of parameters is further reduced by rescaling the time by a factor $\omega_o > 0$ where $|\gamma_0| = \omega_o^2$, and by rescaling the variables a and b, introducing $\tau = \omega_o \bar{\tau}$, $\bar{a} = \rho_1 a$ and $\bar{b} = \rho_2 b$, leading to the ANAET simplified or ANAETs equations

$$\frac{d^2\bar{a}}{d\tau^2} = \epsilon^{-2} \left(-\bar{a} + \bar{b}\bar{a}^3 \right) - \bar{\mu}_6\bar{a}^6 \frac{d\bar{a}}{d\tau} \tag{43}$$

$$\frac{d\bar{b}}{d\tau} = 1 - \bar{\nu}_2 \bar{b}^2 - \bar{a}^2 \tag{44}$$

where in terms of the original parameters

$$\frac{\tau}{t} = \frac{\mu_2}{\delta_0} \frac{\nu_1^2}{\omega_o^2}, \qquad \rho_1 = \sqrt{\frac{\delta_0}{\nu_1}} \tag{45}$$

$$\rho_2 = \frac{\mu_2 \nu_1}{\delta_0 \omega_o^2}, \qquad \epsilon = \frac{\mu_2 \nu_1^2}{\delta_0 \omega_o^3} \tag{46}$$

$$\bar{\mu}_6 = \mu_6 \left(\frac{\omega_o}{\delta_0}\right)^2 \frac{\nu_1}{\mu_2}, \quad \bar{\nu}_2 = \frac{\nu_2}{\nu_1} \left(\frac{\delta_0 \omega_o^2}{\mu_2 \nu_1}\right)^2$$
 (47)

The above suggests that ANAETs has three parameters, but to a significant extent, its behaviour depends on four or possibly five parameters since the fast system governing a(t) has Hamiltonian

$$H_b(q,p) = \frac{1}{2} \left(p^2 + \gamma_0 q^2 - \frac{1}{2} \mu_2 b q^4 \right), \quad q = a, \ p = \dot{a}$$
 (48)

so that, as shown for the ANAC model in Section 2.1, system evolution may depend critically on both initial a and da/dt. Pragmatically, it seems adequate to disregard this caveat in cases where b undergoes a rapid transient, and otherwise to specify only a fourth parameter as the initial value of H, which may be used to parameterise a(0) and $\dot{a}(0)$.

Focusing on the spiking behaviour of exhibited by a(t), a series of calculations exploring the variation of primarily the parameters $\tilde{\delta}_0$, $\tilde{\nu}_2$ and $\tilde{\mu}_6$ was performed. The results show how the number of oscillations can be significantly decreased, see Fig. 5(b) or increased, see Fig. 6.

Importance attaches to the ability to increase the number of oscillations per spike excursion in ANAET. It is observed in the numerical calculations that further increasing $\tilde{\nu}_2$ will lead to yet greater numbers of

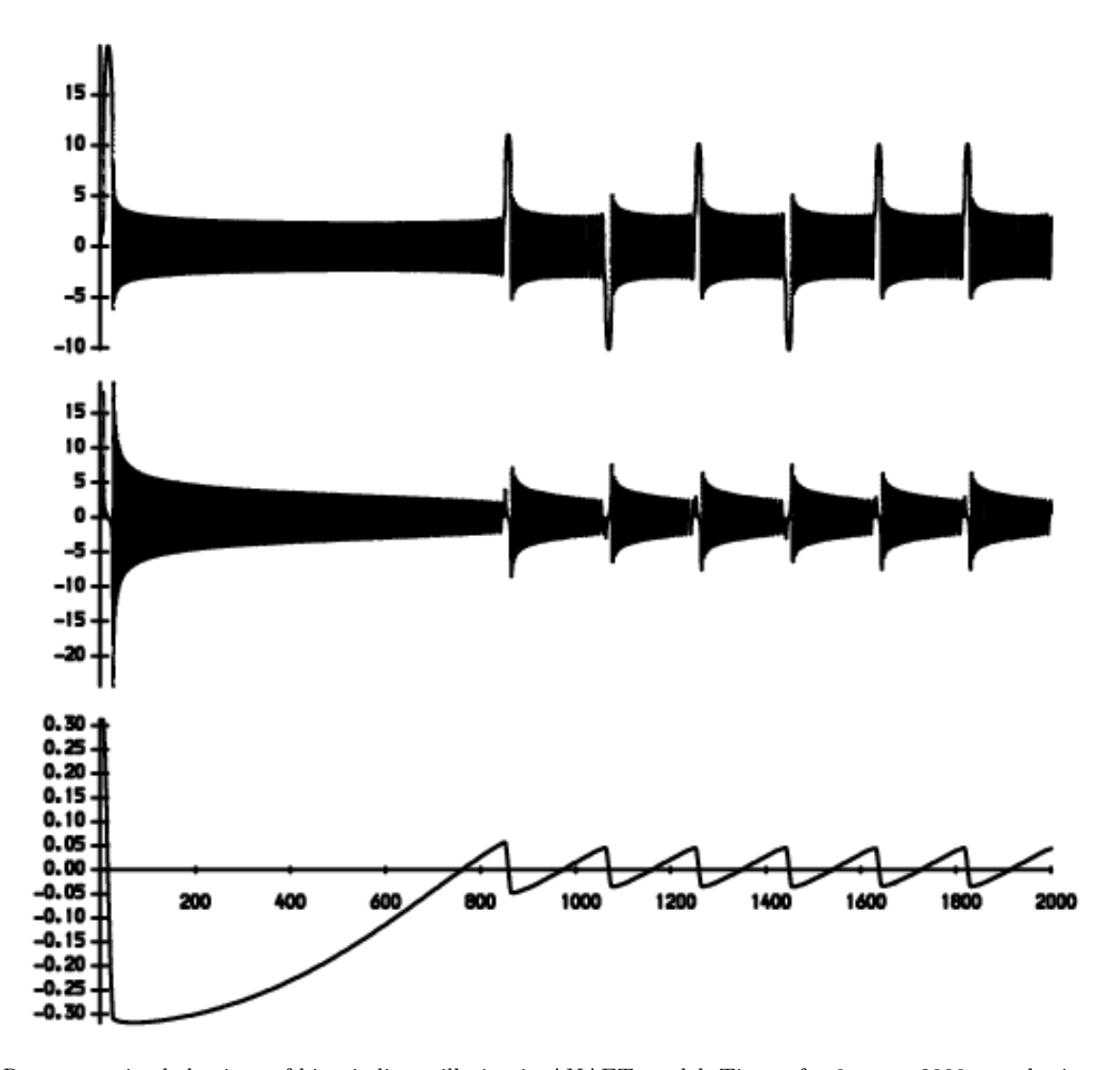


Fig. 4. Representative behaviour of biperiodic oscillation in ANAET model. Time t for 0 < t < 2000 runs horizontally, and time plots of the variables a(t), $\dot{a}(t)$ and b(t) are stacked one above another. Initial conditions a(0) = 0, $\dot{a}(0) = 0.9$ and b(0) = 0.31. Default parameters $\epsilon = 10^{-3}$, $\mu_1 = \tilde{\delta_1} = 0$, $\gamma_0 = \nu_1 = 1$ and $\mu_2 = 2$. $\tilde{\delta_0} = 0.1$, $\tilde{\nu_2} = 5$ and $\tilde{\mu_6} = 0.1$. (See Fig. 5(a) for a shorter time series bringing out the finer detail.)

intermediate oscillations. Fig. 6 shows approximately 300 per spike, about as large a value of this property as it is reasonable to present graphically. However, in addition, the number might also be expected to increase proportionately to $1/\epsilon$. Since the ratio $\tilde{\mu_6}\epsilon^2$ of the coefficients in Eq. (41) does not solely controls the property, the implication is that there is a wide region of parameter space where the number of intermediate oscillations is large, which will likely include situations where this quantity may increase without bound.

Blue-sky Attractor?

This is not the place for a comprehensive analysis of the simplified ANAET model, but in order to appreciate its spiking behaviour better, it is necessary to understand the biperiodic oscillations seen in Figs. 4–6. To this end, it helps to begin with the study of the singular points of ANAETs, although using the notation of Eq. (41) which corresponds to the numerical implementation. These points are given by a=0 and $b = \pm \sqrt{\tilde{\nu}_1/\tilde{\nu}_2}$, and essentially by construction lie on the two branches of a saddle-node bifurcation, with $a=0, b=+\sqrt{\tilde{\nu}_1/\tilde{\nu}_2}$ as the stable equilibrium denoted SE1. The behaviour of a(t) has a fast component which is described by the Hamiltonian $H_b(a,\dot{a})$ of Eq. (48), confined to an 'energy' surface H(0) determined by initial conditions.

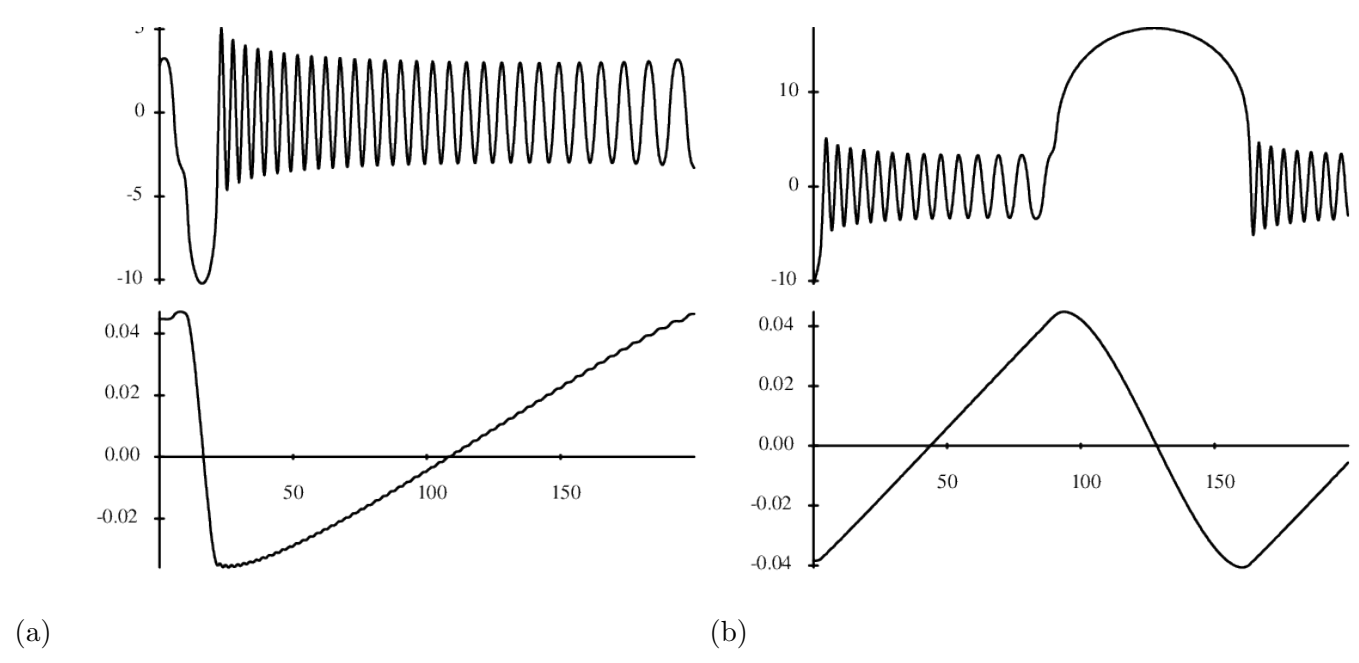


Fig. 5. Different behaviours of biperiodic spiky oscillation in a(t) from ANAET model, plotted over 200 time units after initial transients have decayed, time plots of the variables a(t) and b(t) are stacked one above another. Default parameters $\epsilon = 10^{-3}$, $\mu_1 = \tilde{\delta_1} = 0$, $\gamma_0 = \nu_1 = 1$, $\mu_2 = 2$, $\tilde{\nu_2} = 5$ and $\tilde{\mu_6} = 0.1$, Left (a), short duration spikes between longer interval intervals of bursting at $\tilde{\delta_0} = 0.1$, Right (b), approximately equal duration of spiking and bursting intervals when $\tilde{\delta_0} = 0.01$.

In Section 2.2 constant b was implicitly assumed when studying the properties of the potential $V_b(a)$ that defines H_b , whence it follows that in any plane b = const. > 0, simple closed orbits are found provided $a \leq |a_{bm}|$ where $a_{mb} = \sqrt{\gamma_0/(\mu_2 b)}$, see Fig. 7 for their illustration. When $a > a_{mb}$, the biperiodic orbits become possible. Their features calculated, numerically in the previous section, suggest the existence of the blue-sky attractor described by [Shilnikov and Turaev, 2007, Group IV] with infinite period and infinite length, resulting from an interaction between two distinct periodic cycles. In the case of ANAET, the two cycles would seem to be the two orbits which respectively exit the potential well at $a = \pm \sqrt{\gamma_0/(\mu_2 b)}$.

As the H(0) parameter is increased, the simple oscillation is seen numerically to be replaced by two biperiodic ones. This feature is perhaps not quite what might be expected from [Shilnikov and Turaev, 2007], which would rather imply the merger of two singly periodic ones. Moreover, the apparent distinctness of the two exit orbits may arise only because a simple orbit is more likely to cross the bifurcation threshold when in the regions where orbital speed is least. In addition, since $\mu_6 > 0$ will ultimately cause the simple orbit to decay, strictly speaking the bifurcation is from two biperiodic oscillations to saddle-node, which does not fit so neatly into the blue-sky scenario.

The classification scheme for spiking activity of [Izhikevich, 2007, § 9] seems equally as applicable. This scheme might see ANAET as a 2+1 system, where a defines a 2nd order fast system and b the slow '+1' variable. The technique of plotting the fast variable in planes where the slow variable corresponds to the approach of Section 2.2, showing that the fast oscillation loses stability via a saddle-homoclinic orbit. However for ANAET, the result is not a resting period at the stable equilibrium SE1, but rather a set of small amplitude oscillations because of the absence of effective damping when $|a| \ll 1$. Hence ANAET might be described as a cycle-cycle burster [Izhikevich, 2007, Ex. 19], although there are objections to this classification too, in that b does not very slowly throughout, and the small amplitude oscillations are not generally spiky.

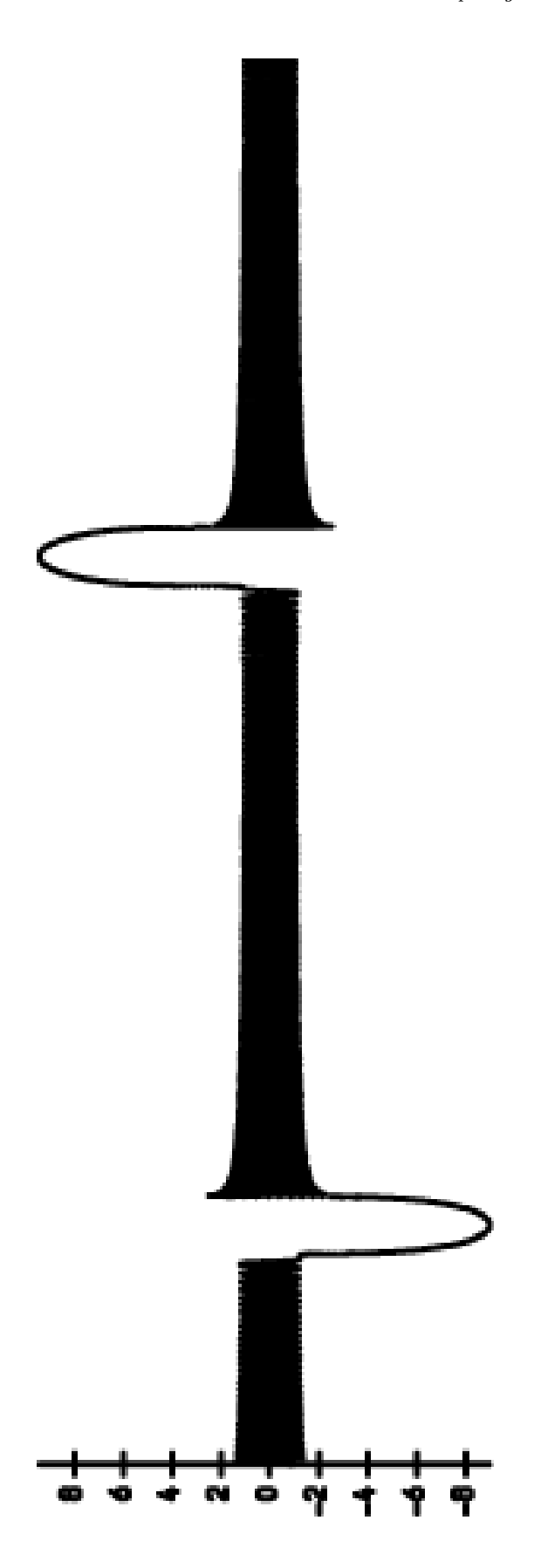


Fig. 6. Long period a(t) solutions of ANAET model, 0 < t < 2000 or $0 < \tau < 2$. Default parameters $\epsilon = 10^{-3}$, $\mu_1 = \tilde{\delta}_1 = 0$, $\gamma_0 = \nu_1 = 1$ and $\mu_2 = 2$. $\tilde{\delta}_0 = 0.15$, $\tilde{\nu}_2 = 1$ and $\tilde{\mu}_6 = 10$.

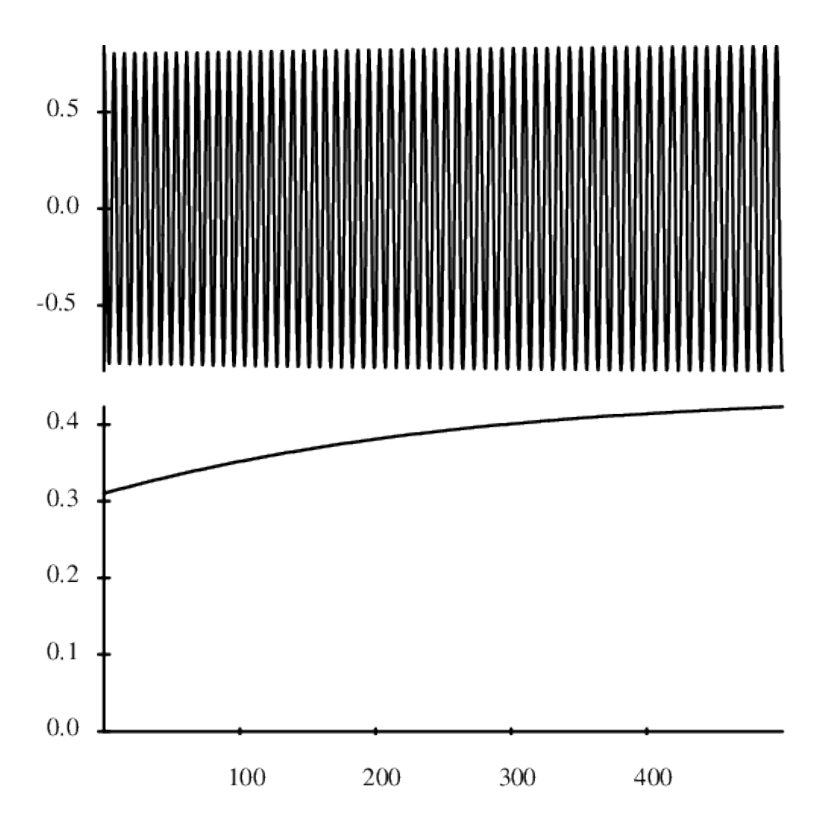


Fig. 7. Representative behaviour of simple oscillation in ANAET model. Time t for 0 < t < 500 runs horizontally, and time plots of the variables a(t) and b(t) are stacked one above another. Initial conditions a(0) = 0.8, $\dot{a}(0) = 0$ and b(0) = 0.31. Default parameters $\epsilon = 10^{-3}$, $\mu_1 = \tilde{\delta_1} = 0$, $\gamma_0 = \nu_1 = 1$ and $\mu_2 = 2$. $\tilde{\delta_0} = 0.1$, $\tilde{\nu_2} = 5$ and $\tilde{\mu_6} = 0.1$.

3. Discussion

The work has discussed spiking activity in systems that may be conceived of as the classical problem of a particle moving in an energy potential, and the coupled evolution of a second, distinct 'background' variable b, where in the case of the ANAET model, the evolution of b changes the form of the potential. The studies of ANAET indicate a (physically) likely mechanism for the production of spiking activity, that might involve a blue-sky catastrophe/bifurcation of the kind described by Shilnikov and Turaev, 2007. Depending on the time spent within a potential well, high frequency spiking behaviour ranges from intermittent to almost continuous, with release from a well of varying depth controlled by the 'background' that evolves on a slow timescale. The ANAET model provides a scenario in which the spikes produced by the ANAC model are to be expected, namely the collapse of a central well to expose a larger, symmetric double well. At the time of escape, the 'particle' appears with negligible motion close to the origin, but considerable potential energy relative to the bottom of the wells. This sets the stage for an exponentially fast motion into the well, which then sees the particle reverse equally abruptly due to the absence of damping in the model. These spikes may be seen distorted into sawtooth-like asymmetry and in some cases dramatically amplified in the behaviour of the background variable, thanks to a third-order one-way coupling in ANAC.

The spiking activity of ANAC, which is generic under the above circumstances, may seem strange when it is realised that the particle motion is described by a Jacobi elliptic function. The impression given by recent works is that these functions resemble sinusoids with squared-off shoulders, whereas the classical work [Whittaker and Watson, 1962, § 22.82] merely invites readers to sketch for themselves Seiffert's spirals on the surface of a sphere. Nonetheless, as shown by [Oldham et al., 2009, p. 641], the Jacobi elliptics do become spiky when their modulus approaches unity, which corresponds to the case of placing a stationary particle near the centre of a symmetric double potential well.

An important feature of the ANAET model is its simplicity relative to other models of spiking and blue-sky catastrophe/bifurcation. Writing the model as a set of three first order equations, the minimal model contains eight terms on the right-hand-side, all multinomial and apart from one, all of order four or less. The seminal Hodgkin-Huxley equations [Hodgkin and Huxley, 1952] for the modelling of spiking in animal neurons are considerably more complex, understandable in an early attempt to fit to experimental data. Nonetheless, apart from the FitzHugh-Nagumo model with 7 terms and two equations [Izhikevich and FitzHugh, 2006], most simplified neuron models are at least as complex as that of [Hindmarsh and Rose, 1984] who give three equations with 11 terms in total added together. In respect of blue-sky catastrophe/bifurcation, [Shilnikov and Turaev, 2007] require 20 multinomial terms or the introduction of exponential functions in some terms, in their third order models. Arguably, and unsurprisingly since it was in part inspired by the work of [Guckenheimer and Holmes, 1983], the ANAET representation of 'blue-sky and spiking' compares favourably in terms of complexity with the Zero-Hopf model presented by [Kuznetsov, 1995, Eq. (8.79)] which treats generic behaviour in the vicinity of the doubly degenerate bifurcation. The cited, more generic system is multinomial, but involves complex variables, which when multiplied out yield a third order system with 13 terms, albeit that none has order more than three.

The approach developed herein, of a particle moving classically in a tightly-coupled evolving potential landscape, is intuitively easy to follow. Aspects of this approach have been noted in textbooks. The last chapter of [Thompson and Stewart, 2002] summarises extensive work on escape from a potential well. Contrastingly, the main emphasis there is on the role of explicit periodic sinusoidal forcing [Thompson and Stewart, 2002, § 16.2] rather than evolving a 'background', their well is described by a *cubic* not quartic potential as herein, and interest attaches to the appearance of chaotic behaviour close to parameters where the blue-sky bifurcation occurs. Although in Section 2.4 the limit of vanishing dissipation appears to be the cause of difficulty in classifying the biperiodic ANAET oscillations, [Wiggins, 2003, § 33] has commented favourably on the more detailed analysis enabled by transforming models of global bifurcations into perturbations of Hamiltonian systems.

Generalisations of the ANAET approach mentioned in Section 1 would seem to be worth exploring, not only for immediate application to nuclear fusion questions, but because they might well have further useful insights to offer, including possibly quantitative estimates of system behaviour, into questions from neuroscience and other fields.

Acknowledgments

I thank my sometime colleague Andrea Murari and student Alasdair Roy for thought-provoking discussions. This work has been carried out within the framework of the EUROfusion Consortium, funded by the European Union via the Euratom Research and Training Programme (Grant Agreement No 101052200 – EUROfusion) and from the EPSRC[grant number EP/W006839/1]. To obtain further information on the data and models underlying this paper please contact PublicationsManager@ukaea.uk. Views and opinions expressed are however those of the author only and do not necessarily reflect those of the European Union or the European Commission. Neither the European Union nor the European Commission can be held responsible for them.

References

- W. Arter. Symmetry constraints on the dynamics of magnetically confined plasma. *Physical Review Letters*, 102(19):195004, 15 May 2009.
- W. Arter. Prior Information for Nonlinear Modelling of Tokamaks. Technical Report UKAEA FUS 553, UKAEA, 2009. https://scientific-publications.ukaea.uk/wp-content/uploads/ UKAEA-FUS-553FINAL.pdf.
- W. Arter. A Solution to the Magnetohydrodynamic Trigger Problem. Technical Report CCFE-R(11)13, UKAEA, 2011. https://scientific-publications.ukaea.uk/wp-content/uploads/CCFE-R1113.pdf.
- A.J. Brizard. A primer on elliptic functions with applications in classical mechanics. *European Journal of Physics*, 30:729, 2009.
- M. Diener. The canard unchained or how fast/slow dynamical systems bifurcate. The Mathematical Intelligencer, 6(3):38–49, 1984.
- S. Gonchenko, A. Kazakov, D. Turaev, and A.L. Shilnikov. Leonid Shilnikov and mathematical theory of dynamical chaos. *Chaos: An Interdisciplinary Journal of Nonlinear Science*, 32(1), 2022.
- I.S. Gradshtevn and I.M. Ryzhik. Tables of integrals, series, and products. Academic Press, 1980.
- J. Guckenheimer and P. Holmes. Nonlinear Oscillations, Dynamical Systems, and Bifurcations of Vector Fields. Springer, 1983.
- J.L. Hindmarsh and R.M. Rose. A model of neuronal bursting using three coupled first order differential equations. *Proceedings of the Royal Society of London. Series B, Biological Sciences*, 221:87–102, 1984.
- A.L. Hodgkin and A.F. Huxley. A quantitative description of membrane current and its application to conduction and excitation in nerve. *The Journal of physiology*, 117(4):500–544, 1952.
- E.M. Izhikevich. Dynamical systems in neuroscience. MIT press, 2007.
- E.M. Izhikevich and R. FitzHugh. FitzHugh-Nagumo model. *Scholarpedia*, 1(9):1349, 2006. http://www.scholarpedia.org/article/FitzHugh-Nagumo_model.
- P.V. Kuptsov, S.P. Kuznetsov, and N.V. Stankevich. A family of models with blue sky catastrophes of different classes. *Regular and Chaotic Dynamics*, 22(5):551–565, 2017.
- Y.A. Kuznetsov. Elements of Applied Bifurcation Theory. Springer, 1995.
- A. Murari, W. Arter, D. Mazon, M. Gelfusa, V. Ferat, and JET-EFDA Contributors. Symmetry based analysis of macroscopic instabilities in Tokamak plasmas. Technical Report PR(11)07, JET-EFDA, 2011. https://scipub.euro-fusion.org/wp-content/uploads/2014/11/EFDP11007.pdf accessed 21/9/24.
- K.B. Oldham, J. Myland, and J. Spanier. An Atlas of Functions: with Equator, the Atlas Function Calculator. Springer, 2009.
- K. Radhakrishnan and A.C. Hindmarsh. Description and Use of LSODE, the Livermore Solver for Ordinary Differential Equations. Technical Report UCRL-ID-113855 (NASA RP-1327), Lawrence Livermore National Laboratory, 1993. URL http://gltrs.grc.nasa.gov/cgi-bin/GLTRS/browse.pl?2003/RP-1327. html.
- Sanaullah, S. Koravuna, U. Rückert, and T. Jungeblut. Exploring spiking neural networks: a comprehensive

- analysis of mathematical models and applications. Frontiers in Computational Neuroscience, 17: 1215824, 2023.
- A. Shilnikov and D. Turaev. Blue-sky catastrophe. *Scholarpedia*, page 2(8):1889, 2007. http://dx.doi.org/10.4249/scholarpedia.1889.
- J.M.T. Thompson and H.B. Stewart. *Nonlinear Dynamics and Chaos, 2nd Edition*. John Wiley & Sons Inc, 2002.
- E.T. Whittaker and G.N. Watson. A Course of Modern Analysis, 4th Ed. Cambridge University Press, 1962.
- S. Wiggins. Introduction to Applied Nonlinear Dynamical Systems and Chaos 2nd Ed. Springer, New York, 2003.
- M. Yamada. Magnetic reconnection. Princeton University Press, 2022.